Journal of Structural Geology, Vol. 10, No. 3, pp. 239 to 247, 1988
Printed in Great Britain

0191-8141/88 $03.00 + 0.00

Analysis of the relationship between displacements and dimensions of faults

JOHN J. WALSH and JUAN WATTERSON

Department of Geological Sciences, University of Liverpool, P.O. Box 147, Liverpool L69 3BX, U.K.

(*Received* 29 *January* 1987; *accepted in revised form* 15 *September* 1987)

Abstract—Displacement gradients on single fault surfaces are a function of the maximum displacement on a fault and the dimensions of the fault surface. Data on the maximum lateral dimensions (widths) and maximum displacements on normal faults and thrusts, with maximum displacements from 4 mm to 40 km, are used to derive an expression relating width, displacement and material properties. The basis of this expression is a fault growth model in which width is proportional to the square root of displacement. Width/displacement ratios vary systematically with the size of a fault from values of *ca* 30,000, which are characteristic of a single slip event, to about 10 in the case of thrusts with displacements of 40 km. Rocks from which the fault data are derived have a likely range of shear moduli from *ca* 0.1 to *ca* 30 GPa, which is sufficient to account for the range of data.

Data on widths and maximum displacements of 308 fault traces recorded on British coalmine plans are shown to be consistent with variation of shear modulus of about half an order of magnitude. Data on 58 further fault traces are shown to be consistent with the fault growth model. Synsedimentary faults may have growth curves characteristically different from those of other faults.

It is suggested that the increase in dimensions of a fault is a postseismic process of subcritical crack propagation for which the significant material property is fracture toughness.

INTRODUCTION

DISPLACEMENT on a single fault surface ideally decreases to zero in all directions from a point of maximum displacement, except where the fault intersects a free surface or where displacement is transferred to a splay or to an intersecting fault. In the simplest cases the fault surface is an ellipse bounded by the zero displacement contour or tip-line loop (Fig. 1) (Rippon 1985, Barnett *et al.* 1987). The fault width (W) is defined as the maximum dimension of the surface in a direction normal to the slip direction and the fault length is the maximum dimension parallel to the slip direction. The size of a fault trace on a map can always be referred to as the length of the fault trace, because it is two dimensional. The radius (R) of a fault is half of either the width or the length: as most of the available data is for fault widths, the term radius here refers to half of the width, unless stated otherwise. Displacement (D) refers to the displacement accumulated throughout the active life of the fault and slip (u) refers to the slip occurring during a single seismic event or cycle. The displacement gradient on a fault is a measure of the rate at which displacement changes along the fault plane in a specified direction. A knowledge of the usual range of gradients can be used either for testing the geometric compatibility of a fault interpretation or for extrapolating a fault beyond the area for which data are available. The characteristic displacement gradient of a fault is given by the ratio D/R, but as these values are less than 1 it is often more convenient to refer to the reciprocal of the displacement gradient (R/D). Elliott (1976) suggested that a linear relationship between R and D is likely and that the characteristic value of the R/D ratio is *ca* 7, and this value has become accepted as the norm (Coward & Potts 1983). It is shown here that the relationship between D and R, for a variety of faults, is non-linear and that R/D values range from 5 to 1000. We also consider the displacement gradients, d/r, along fault traces (i.e. chords of the fault ellipse), where r is half a chord and d is the maximum displacement on the fault trace (Fig. 1). Because tip-line loops are ideally elliptical, the displacement gradient on a fault also varies with the direction of the radius or chord along which it is measured. The data available for analysis is almost exclusively for fault radii or chords parallel to the widths of faults (i.e. normal to the slip direction), which on the evidence of contoured displacements from coalfield faults (Rippon 1985, Barnett *et al.* 1987), characteristically have displacement gradients about a half of those along the lengths of faults.

The purpose of this contribution is to give an assessment of characteristic displacement gradients on a variety of faults, to give a quantitative analysis of the factors

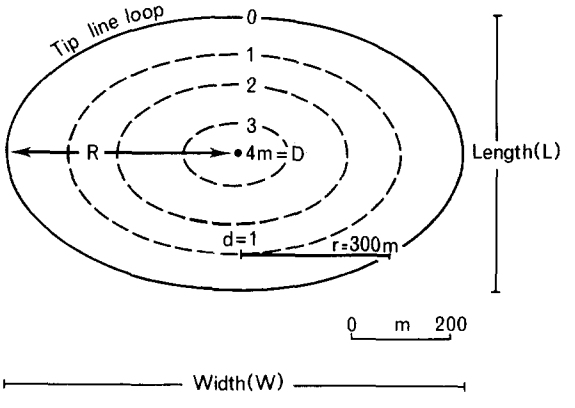

Fig. 1. (a) Schematic diagram of contoured displacements on a fault surface with maximum displacement (D) at the centre of the fault and with the tip-line loop corresponding to the zero displacement contour. Radius (R) is half the width. Displacement (d) is the maximum displacement along a chord of half-width (r).

which determine these gradients, and to present and interpret displacement gradient data from 366 fault traces from British coalfields and elsewhere. The faults considered are single intraplate faults contained wholly within the seismogenic layer, and are not part of a larger scale linked fault system.

THE GROWTH MODEL

A systematic relationship between the widths and maximum displacements on single faults has been previously demonstrated (Watterson 1986) and the relationship has been interpreted in terms of a fault growth model. The fault growth model gives rise to the expression:

$$D = W^2/P, \quad (1)$$

where D = maximum displacement on the fault;
W = maximum dimension of the fault surface in the direction normal to the slip direction;
P = variable related to rock properties.

This section provides an evaluation of, and derives an expression for, P, following a brief description of the fault growth model and the available data.

A systematic relationship between maximum displacement and fault width is evident from the data shown in Fig. 2. The data are for normal faults and thrusts for which the maximum displacement has been determined either from well data, or by contouring of displacements (Rippon 1985), or in some cases (mid-ocean ridge, Icelandic and thrust data) by assuming that the maximum displacement is at the surface. Sources of the data are given in Watterson (1986) and Barnett *et al.* (1987). Data for faults in Quaternary lacustrine sediments (Muraoka & Kamata 1983) list fault length as opposed to width (see Fig. 1); these faults are considered in a later section. Additional data include the field containing coalfield fault traces and a single datum representing the Lost River Fault (Stein & Barrientos 1985); these data are considered in detail in later sections. Also shown are two lines which bound the data distribution and have a slope of 2, which is appropriate to the growth model (see equation 1). The best-fit line has a slope of 1.58 but, as is shown later, the data will not ideally lie along a single line and a regression line has little significance.

The data define a linear band corresponding to variation in fault width of approximately one order of magnitude for a given displacement (Fig. 2). The linear trend of the data on the log–log plot is a reliable indication that the data represent a growth sequence, i.e. that the larger faults have grown in a series of stages represented by the smaller faults. A significant progressive change is seen in the W/D values, which vary from 2000 to 10 with increasing size of fault. It is clear that the band containing the data does not lie at 45° to the axes of the plot (a slope of 1) and therefore the relationship between displacement and width is non-linear, i.e. an increase in D corresponds to a much smaller proportional increase in W, as expressed by equation (1). This relationship contrasts with the linear relationship between the width of a fault and the amount of slip during a single seismic event (Kanamori & Anderson 1975, Scholz 1982): the slip/width ratio for large intraplate earthquakes is about 6×10^{-5} (Scholz *et al.* 1986), based on the assumption of a circular fault. The corresponding slip/width ratio for an elliptical fault, 3×10^{-5}, is shown in Fig. 3, plotted with the bounding lines of Fig. 2 and a 'standard' fault curve (midway between the bounding lines). Although for convenience

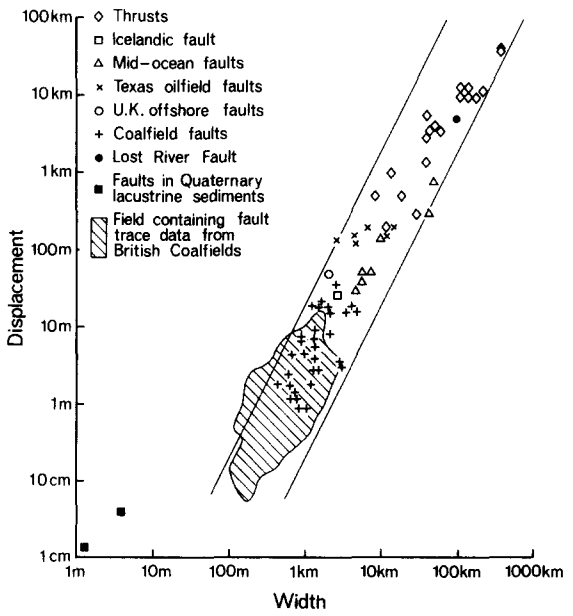

Fig. 2. Logarithmic plot of width against maximum displacement for faults. Continuous lines have a slope of 2, as appropriate to the growth model (see text for details). Shaded area denotes the field containing data points for fault traces in British coalfields (see Fig. 5).

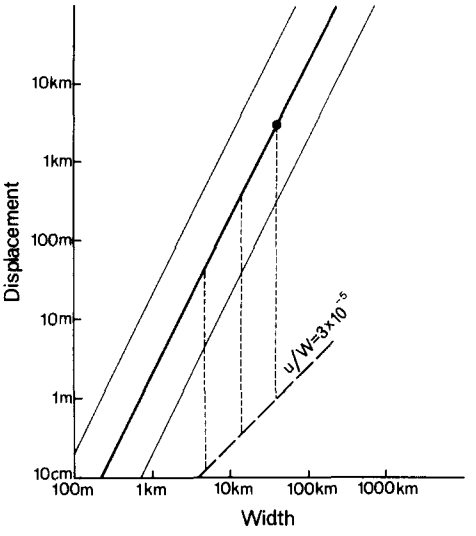

Fig. 3. Logarithmic width vs maximum displacement plot with light solid lines representing the bounding growth curves for the data in Fig. 2 and heavy solid line representing the 'standard' growth curve for the same data (see text for details). The heavy broken line is the representative locus of single slip events on an active fault with typical constant slip/width ratio of 3×10^{-5}. Vertical broken lines represent tie lines relating slip to total displacement at three stages during the growth of a fault lying on the 'standard' growth line. The black circle represents the final maximum displacement and the width of the fault.

slip is taken as coseismic, it refers to all slip taking place in a single earthquake cycle which also includes interseismic, preseismic and postseismic phases (Kasahara 1981): the difference is not significant for current purposes. For aseismic faults the equivalent time is some period of hundreds or thousands of years, which is long enough for short-term fluctuations in the rates of stable sliding to be smoothed out.

The tie lines in Fig. 3 show that with increasing cumulative displacement on a fault, both the fault width and the amount of slip in a single event also increase if growth parallels the 'standard' curve. It follows that the amount of slip must increase with each successive slip event. It has been shown (Watterson 1986) that the data distribution is consistent with a constant slip increment throughout the active life of a fault, i.e. an arithmetic series of slips. In other words, the width of a fault increases by a constant amount, as opposed to a constant proportion, with each successive event. Growth models in which width increases by a constant proportion with each slip event are characterized by a linear relationship between D and W which is not consistent with the data.

The arithmetic growth model leads directly (Watterson 1986) to the relationship between displacement and width given in equation (1), which can also be expressed as:

$$\log P + \log D = 2 \log W.$$

On a log–log plot the growth curve corresponding to this expression is a straight line with a slope of 2 (i.e. at an angle of 63.44° to the width axis), which is the slope of the bounding lines and of the 'standard' growth line (Fig. 3). The position of a growth line varies with the value of P (Watterson 1986), which is assumed to be constant during growth of a single fault.

Faults with the same displacement may have widths differing by as much as an order of magnitude, therefore the data distribution is more realistically described by the two bounding growth curves (Fig. 2), rather than by the 'standard' growth curve. Of the many possible contributions to this spread, which include inaccurate data, the most significant is thought to be variation in material properties.

Material properties

For a fault growing according to the arithmetic growth model (see Appendix)

$$u_n = a \times n, \tag{2}$$

where u_n is the final slip, a is the increment of slip increase between successive events and n is the (large) number of slip events.

For a single earthquake slip event, stress drop ($\delta\sigma$) and shear (or rigidity) modulus (G) are related to u_n and to the fault radius ($R = W/2$) by the following expression (Kanamori & Anderson 1975)

$$\delta\sigma = (7 \times \pi \times G/16) \times u_n/R, \tag{3}$$

where $7 \times \pi/16$ is the shape factor for a circular fault. Combining equations (1)–(3); (see Appendix)

$$W^2 = D \times ((7 \times \pi \times G)/(16 \times \delta\sigma))^2 \times 8a \tag{4}$$

$$P = ((7 \times \pi \times G)/(16 \times \delta\sigma))^2 \times 8a. \tag{5}$$

Equation (5) demonstrates that P is dependent on the variables G, $\delta\sigma$ and a.

Shear modulus is proportional to fault width and inversely proportional to the square root of D (equation 4). If shear modulus were the only variable, the difference between the bounding growth curves would correspond to an order of magnitude variation in G; values of 3 and 30 GPa have been assigned to the upper and lower bounding curves, respectively. Actual values of G for the faults plotted in Fig. 2 could vary to this extent. The higher value (30 GPa) is typical of metamorphic and felsic igneous rocks (Birch 1966) and is the assumed crustal value usually used in earthquake seismology. A shear modulus of 3 GPa is about that expected for a soft sandstone in the British Coal Measures; hard sandstones in coalfields have shear moduli of about 12 GPa and shales about 1 GPa (C. Morris personal communication, 1985). The coalfield and oilfield faults plot mostly within the range corresponding to values between 3 and 10 GPa; the 'standard' growth curve (Fig. 3) corresponds to a shear modulus of 9.5 GPa.

The two faults in Quaternary deposits (Muraoka & Kamata 1983) are distinct from the other faults plotted (Fig. 2) and on the basis of the values assigned to the bounding curves, are consistent with values of shear modulus of 0.1–0.2 GPa. No data are available for faults of similar size in other types of rock.

Variations in stress drop and slip increment relative to variation in the shear modulus are best illustrated by reference to a model fault. The amounts by which each parameter would need to vary to displace the plotted position of the model fault from one bounding curve to the other can be determined. The fault plotted on Fig. 3 has the following values:

$W = 40$ km $\quad G = 30$ GPa
$D = 3$ km $\quad u_n = 3.64$ m

from which the following values can be derived:

$u/R = 1.82 \times 10^{-4} \quad a = 2.2$ mm
$\delta\sigma = 7.5$ MPa (75 bars) $\quad n = 1654.$

Because the stress drops derived for earthquakes are usually calculated on the basis of an assumed value for G of 30 GPa and because these two parameters are directly proportional, 30 GPa is used instead of 9.5 GPa which would be consistent with the data. Stress drop is directly proportional to fault width (equation 4), so that an order of magnitude variation, 2.4–24.7 MPa, would be required to shift the plotted point from one bounding curve to the other. This variation in stress drop is slightly larger than the probable variation in stress drops on intraplate faults, which mostly range between 3 and 13 MPa (Kanamori & Anderson 1975). For constant G, variation in stress drop is determined by variation in the slip/radius ratio, which is believed to vary with frictional properties of the fault surface (Scholz *et al.* 1986).

There is no observational data for any fault from which values of the slip increment (a) can be derived directly. If stress drop and shear modulus are constant, u/R is constant and u_n is fixed for a fault of given W; a is then inversely proportional to D and n. The change from one bounding curve to the other spans two orders of magnitude variation in D, which also requires two orders of magnitude variation in n. The value of n for a fault is given by the ratio of age to recurrence interval; intraplate earthquakes have recurrence intervals greater than 10,000 years (Scholz *et al.* 1986). The range of ages of faults 40 km wide is not known. Therefore, in view of the lack of observational data, the possibility cannot be excluded that the spread of data between the bounding curves is due to variation in slip increment size. However, as the expected range of values for G is sufficient to account for the data distribution, variation in slip increment size and in stress drop are provisionally regarded as being of secondary importance.

The Lost River Fault

A demonstration of the significance of the variables in equations (2) and (4), using data appropriate to the Lost River Fault, is given below. The data for this fault are probably more comprehensive than on any other active normal fault, and have been derived from seismic, long-term geodetic and geological investigations (Barrientos *et al.* 1985, Stein & Barrientos 1985).

The Lost River Fault lies in an area of Basin and Range structure in central Idaho. Displacement began in the Pliocene (*ca* 3.5 Ma; Ruppel 1982) or in the latest Miocene to early Pliocene (4–7 Ma; Scott *et al.* 1985) along most of its surface trace, but there are indications of activity in mid-Cenozoic times. This planar normal fault extends to a depth of about 13 km with a dip of 45°. On the basis of geomorphic features and ages of latest movements, seven segments have been distinguished along the 100 km long fault trace. Central segments have higher cumulative displacement than distal segments. A maximum vertical displacement of 3.0–3.5 km, corresponding to a dip-slip displacement of up to 5 km, has been estimated (Scott *et al.* 1985, Stein & Barrientos 1985).

Coseismic activity associated with the 1983 Borah Peak earthquake was restricted to the central and northern part of this fault, with a maximum coseismic slip of 2.1 m along the segment of highest cumulative displacement (Scott *et al.* 1985) and a slip direction pitching 65° (Barrientos *et al.* 1985). Comparison of earthquake and geologic data however, suggest that an additional 1.5 m of footwall elevation should be attributed to interseismic deformation associated with the Borah Peak earthquake cycle. Estimates of repeat times for earthquakes along central segments of the Lost River Fault vary considerably, but since at least three post-15,000 BP events have occurred (Wallace 1985), 4000 years is used.

The values used for the various parameters are:

W = 100 km $\quad G$ = 30 GPa
D = 5 km $\quad u_n$ = 3.6 m.

From equation (3), the stress drop for each earthquake cycle along the Lost River Fault is 3 MPa, which is within the usual range of stress drops for intraplate earthquakes.

From equation (4), a = 0.13 cm
and from equation (2), n = 2777.

With an estimated repeat time for major events of 4000 years, 2777 events would correspond to an active life of 11.1 Ma. The cumulative displacement associated with this fault at 7.0 Ma BP would have been only 684 m, and at 3.5 Ma would have been 2345 m, i.e. 85% of the displacement would be latest Miocene or later, as reported by Scott *et al.* (1985). The total shear strain (D/W) associated with the Lost River Fault is 0.05, which corresponds to a ductile shear strain rate of 1.43×10^{-16} s^{-1}. Although the assumed and calculated values of fault parameters are internally consistent, they are not necessarily correct but, using equations (1), (2) and (4), the effect of different assumptions on fault radius (R) and displacement (D) can be tested.

FAULT TRACE DATA

The data plotted in Fig. 2 represent maximum values of both displacement and width for each fault. In many circumstances, data are available as fault traces on a surface or subsurface map with no additional information. In such cases the fault trace is a chord of the fault surface ellipse at an unknown distance from the centre (Muraoka & Kamata 1983). With increasing radial distance from the fault centre, the position of a fault trace (or chord) on the width/displacement plot changes, indicating a marked decrease in the displacement gradient on the chord (Fig. 4). Values of d and $2r$ (see

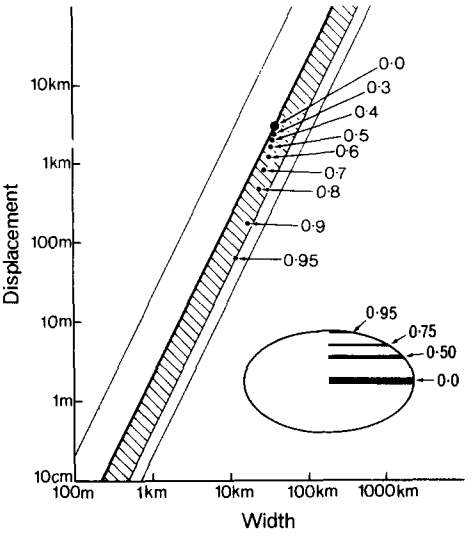

Fig. 4. Logarithmic width vs maximum displacement plot with bounding and 'standard' growth curves as in previous figures and large black circle representing the same fault as in Fig. 3. Smaller circles define the locus of points representing values of chord lengths and of maximum displacement on chords at progressively greater distances from the centre of the fault as given by values of radial distance. Radial distance is the distance from the fault centre, along the length radius, expressed as a fraction of the length radius as shown in inset. Assumed displacement distribution on the fault surface from Walsh & Watterson (1987).

Fig. 1) are plotted for chords progressively further from the centre of the fault and the shaded band indicates the expected range of divergence from a selected growth curve; equivalent to a change of width about 2.3 times for radial distances from 0.0 (fault radius) to 0.95 (see insert, Fig. 4). The displacement gradient along a fault radius is non-linear (Walsh & Watterson 1987) and the appropriate function has been used to calculate the changes on the width/displacement plot with increase in radial distance.

Coalfield data

Data from 308 fault traces recorded on mine plans from British coalfields are plotted in Fig. 5, together with data representing 58 fault traces from other sources. The coalfield faults were selected according to the following criteria: (i) the fault trace terminates in worked ground; (ii) a maximum displacement is identifiable on the trace, either because it is flanked by two lower readings or by interpolation over a short distance between the two highest readings on the trace; (iii) there is no intersection with another fault and no obvious interference with adjacent faults. Each sample plotted represents half a complete trace and in some cases two samples are available from a single fault trace, so that 518 points are plotted from the 308 faults. The half-lengths of the traces have been doubled for plotting. The fault traces are from areas where seam dips are less than 15° and therefore all traces represent horizontal or sub-horizontal chords on the fault planes. Most of the faults have normal throws and are tectonic in origin, but some may represent compaction faults or growth faults which cannot always be distinguished on mine plans.

The displacement measurements in all cases are of vertical displacement, or throw, and have not been corrected to total displacement. Fault dips in the East Pennine coalfield, from which most of the data are derived, average 69° but dips of the individual faults sampled cannot be determined. The most significant source of error is believed to be where the displacement is partly accommodated by ductile drag (Walsh & Watterson 1987).

In most cases, only the displacement on the fault discontinuity is recorded on the plans and therefore some of the maximum displacements are too low. However, there are indications that drag is less important at points of maximum displacement than elsewhere on a fault (Walsh & Watterson 1987). Faults are terminated on mine plans where they become insignificant for mining purposes, i.e. the throw is about 10 cm; it has been shown (Walsh & Watterson 1987), that 50 m should be added to a recorded fault radius to obtain the true value and this has been done for data shown in Fig. 5. This addition is probably too little for chord data because displacement gradients along chords are lower than along radii. The uncertainty is proportionally greater on small faults.

Coalmine plans represent a fault trace within a coal seam but the length of the trace may be different from

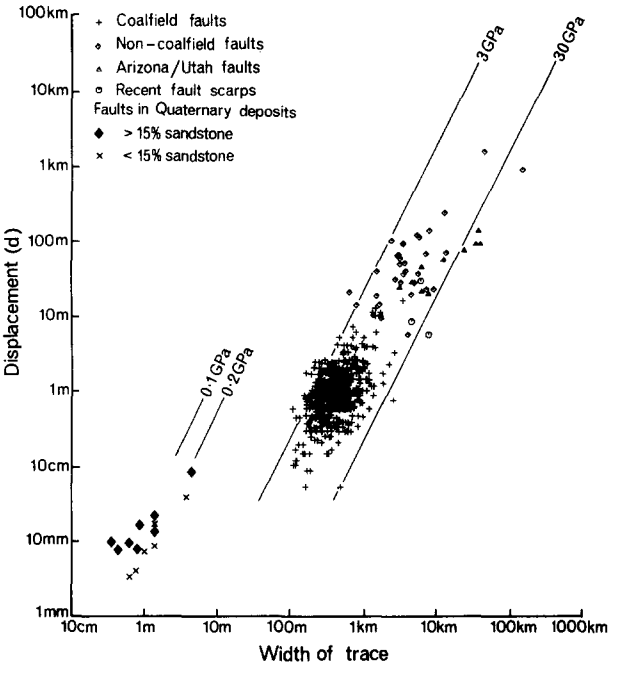

Fig. 5. Fault trace data for British coalfield (n = 518) and data from other sources (n = 58); see text for details. Bounding curves are those shown in previous figures. Estimated values of shear moduli for individual growth curves are given.

that in rocks of different material properties above and below the seam. The shear modulus relevant to the data may therefore be different to that of the sedimentary succession as a whole. About one third of the spread of data normal to the growth curve can be accounted for by the geometry of chord data. As the data are spread downwards from the growth curve (see Fig. 4), only the growth curve representing lower shear modulus coalfield faults will remain well defined; this curve, bounding the upper left of the concentration of data points (Fig. 5), corresponds to a shear modulus of 3 GPa. Assuming that the chords sampled have radial distances of less than 0.95, the distribution of data could be accounted for by a variation in shear modulus of about half an order of magnitude.

Other fault trace data

Displacement/width data from fault traces of 59 normal faults and a single thrust have been derived from published field, mine and seismic data (Table 1). Absolute displacement (d) has been calculated for faults with dips shallower than 60° and others for which accurate dip values are available. The remaining faults (n = 35) have dips which are greater than 60° and the vertical displacements plotted are at most 13.5% less than the absolute displacement. All fault traces plunge at less than 20° and usually represent sub-horizontal (less than 10°) chords on fault planes. These data and the coalfield fault traces are plotted together in Fig. 5 and lie within a band sub-parallel to the bounding growth curves of Fig. 2. As would be expected from chord data geometry, fault trace data are more scattered than the data shown in Fig. 2.

Table 1. Age, location and sources of fault trace data (n = 60)

Age and location	Source	Details
Namurian, Buxton, U.K.	Aitkenhead (1985)	Normal (3,f)
Cenozoic, Arizona/Utah, U.S.A.	Babenroth & Strahler (1945)	Normal (6,f)
Recent, Arizona/Utah, U.S.A.	Babenroth & Strahler (1945)	Normal (3,f)
Cretaceous, Wyoming, U.S.A.	Beck (1929)	Normal (3,fw)
Precambrian–Palaeozoic, Illinois, U.S.A.	Bond *et al.* (1971)	Normal (1,f)
Basal Coal Measures, East Midlands, U.K.	Brunstrom (1963)	Normal (1,m)
Mesozoic, Malmesbury, U.K.	Cave (1977)	Normal (1,f)
*Upper Carboniferous, Ruhr, Germany	Drozdzewski (1980)	Normal and thrust (2,m)
Mid-Dinantian, Bellingham, U.K.	Frost & Halliday (1980)	Normal (2,f)
Westphalian, Derbyshire, U.K.	Frost & Smart (1979)	Normal (1,m)
Cenozoic, Arizona/Utah, U.S.A.	Huntoon (1974)	Normal (1,f)
Upper Eocene, Austria	Janoschek & Gotzinger (1969)	Normal (1,s)
*Tertiary, California, U.S.A.	Mayuga (1970)	Normal (–oblique) (4,sw)
*Quaternary, Japan	Muraoka & Kamata (1983)	Normal (14,f)
*Tertiary, Niger Delta	Nelson (1980)	Normal (2,s)
Pennsylvanian, Kansas, U.S.A.	Reeves (1929)	Normal (3,fw)
Permian, Australia	Shepherd & Burns (1978)	Normal (1,f)
Cenozoic, Arizona/Utah, U.S.A.	Shoemaker *et al.* (1978)	Normal (3,f)
*Cretaceous, Louisiana, U.S.A.	Teas (1929)	Normal (4,fw)
*Paleocene, Oman	Tschopp (1967)	Normal (1,swf)
Paleocene, Ekofisk, North Sea	Van den Bark & Thomas (1980)	Normal (1,s)
Miocene, Indonesia	Verdier *et al.* (1980)	Normal (2,s)

Additional details refer to fault type (normal, thrust, oblique) and (in brackets) the number of faults and data type (f—field, s—seismic, m—mine, w—well), * denotes those faults for which the angle of dip is known.

The data (Fig. 5) include 10 Cenozoic normal faults from North Arizona and South Utah (Babenroth & Strahler 1945, Huntoon 1974, Shoemaker *et al.* 1978). Where there is stratigraphic control, these faults are post-Laramide, i.e. post-Eocene (Shoemaker *et al.* 1978). The four largest faults, at least, result from renewed movement on Precambrian faults. The relatively high W/D ratios of these faults, which plot to the right of the right-hand bounding curve (Fig. 2), may be characteristic of faults formed by basement reactivation, because the tip-lines within the basement are not pinned by intact rock. There is also some evidence for reactivation along the remaining non-coalfield fault which plots to the right of the right-hand bounding curve (Bond *et al.* 1971).

Synsedimentary faults are characterized by an upward decrease in displacement of syn-faulting layers and increased stratigraphic thickness in the hangingwall (Barnett *et al.* 1987). If the rate of sedimentation matches the long-term displacement rate, the maximum surface expression of the fault is a scarp produced by a single slip event, which would plot on the earthquake curve (Fig. 3). The displacement–width characteristics of a fault measured on a given syn-faulting layer will grow along a curved locus between the earthquake curve and the 'standard' growth curve (Fig. 6). The locus is such that the difference between the displacement of a syn-faulting layer and the maximum displacement is constant; on a log–log plot, however, the positions of the fault as measured at a particular layer and at the level of maximum displacement plot closer together as the fault grows. For faulting characterized by very low sedimentation rates relative to displacement rates, the surface expression will be a fault scarp the dimensions of which will grow along the same curved locus; this feature is shown in Fig. 6 for one of the recent fault scarps of Fig. 5. Faults measured in synsedimentary horizons will ideally have growth curves which are steeper than the 'standard' growth curve, and synsedimentary faults may plot in the region below that occupied by other faults. Actual faults may show characteristics intermediate

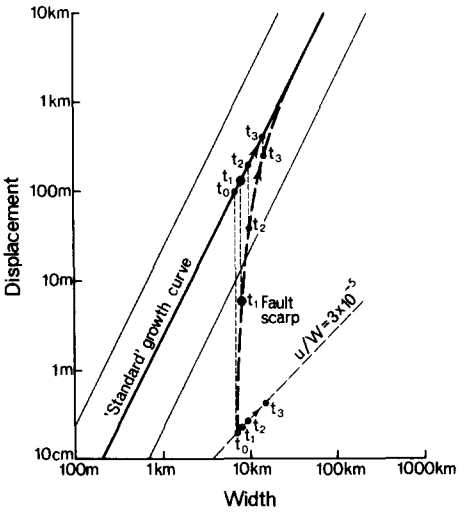

Fig. 6. Logarithmic plot of width vs displacement showing the relationship between the growth curve describing the maximum dimensions and displacements of a synsedimentary fault (heavy solid line) and the growth curve (heavy broken line) defined by fault traces on syn-faulting depositional layers (see text for details). Subsurface measurements at the level of maximum displacement would show the fault lying on a normal growth curve, here taken as the 'standard' growth curve. The heavy broken line represents the growth curve for a syn-faulting depositional layer which was first faulted at time t_0. In areas of very low sedimentation rates (i.e. approaching zero) the growth of fault scarps follows this growth curve; the solid circle at time t_1 on this curve is one of the recent scarps shown in Fig. 5. Vertical broken lines are tie lines joining the growth curves of the fault as seen at the two different levels (t_0—first slip increment displacing most recently deposited layer; t_1—present; t_2 and t_3—projected future growth). The displacements of syn-faulting depositional layers may lie anywhere between the normal growth curve and the locus of single slip events.

between the two specific cases considered; scarp erosion is another potential variable.

Fourteen of the data points in Fig. 5 not included in the foregoing discussion represent fault traces given by Muraoka & Kamata (1983); the data are for chords parallel to the lengths of the faults rather than the widths and the two faults plotted in Fig. 2 are included. The faults occur in Quaternary lacustrine deposits in which fairly hard and compact diatomaceous siltstone is the dominant lithology, with subordinate layers of sandstone and tuff which are commonly soft and loosely compacted. In Fig. 5 two types of fault are distinguished; those intersecting layers with 0–15% sandstone and those which intersect layers with 15–53% sandstone. On the basis of the stress drop equation (equation 3) Muraoka & Kamata (1983) suggest that the shear modulus of the siltstone is more than twice that of the other rocks. This assessment was made by assuming that the faults were the products of single slip events (therefore $D = u$); this is a reasonable assumption for these small faults. The two groups of faults show a trend which, although not inconsistent with an arithmetic growth curve, could equally well be fitted to a geometric growth curve with a slope of 1. On the basis of the shear modulus values assigned to the bounding curves, the shear moduli for the two groups of faults from Japan would be 0.2 GPa for the more competent siltstones and 0.1 GPa for the sandstones. The shear modulus of a densely packed subangular medium sand is given by Lambe & Whitman (1969) as 0.096 GPa.

DISCUSSION

The arithmetic fault growth model incorporates no explanation for fault growth. The dislocation on a fault resulting from a single slip event can be accommodated by the elastic strains in the surrounding rock volume. If these elastic strains are relaxed into permanent strains before the next slip event there is, *a priori*, no reason why this next event should not be an exact repetition of the preceding event with no change in fault dimensions. If this were the case, the systematic relationship between D and W would not occur. Relaxation of elastic strains undoubtedly does occur because the strains necessary to accommodate the cumulative displacement on a large fault are much too high to be accommodated elastically (Watterson 1986). Fault growth would be necessary if some of the elastic strain imposed during one slip event still remained when the next event took place, otherwise successively higher elastic strains would be imposed. Fault growth would then require smaller u/W ratios as a fault grew larger, and hence lower stress drops on larger faults, which is not the case. Growth controlled by the amount of elastic strain relaxed since the previous slip event would not produce a systematic relationship between D and W.

The most unexpected feature of the growth model is that the slip increment (a) is independent of the size of the fault; this characteristic represents a very tight constraint on possible mechanisms for fault growth.

The fault growth model requires that the ratio between the amount of slip and fault width is a constant for all slip events on a single fault, i.e. stress drop is constant (see equation 3). This condition means that slip always occurs when the shear stress on a fault reaches a fixed critical value and ceases when the amount of slip is sufficient to have reduced the stress to another fixed value. Stress drop varies only within narrow limits on all faults of a single type (Scholz *et al.* 1986) and the variation on a single fault is likely to be minimal, although there are no data to support this conclusion.

Given this assumption the stress distribution in the fault volume following each slip event, including the crack tip stresses, will be identical except for scale. Throughout most of the fault volume these stresses, or elastic strains, will be relaxed by permanent straining before the next slip event occurs. Along the tip-line of the fault however, where the highest elastic strains exist, relaxation can be effected by sub-critical fracture propagation (Das & Scholz 1981). It is usual in the analysis of fracture mechanics for the boundary conditions to include the condition of constant stress, which requires propagation of the fracture to be accompanied by relative displacement of the fracture surfaces. In experimental work this condition is met by an apparatus which imposes constant loading of the specimen. In such cases the fracture propagation is always described by an expression which includes crack length as a variable, e.g. $k \propto L^{1/2}$, where k is the stress intensity factor and L is the crack length (Das & Scholz 1981). Under these conditions, identical stress distributions on cracks of different size will always lead to greater crack extension on long cracks than on short cracks. This relationship is inconsistent with the arithmetic growth model. However, there may be no fracture propagation during seismic slip on a pre-existing fracture and the propagation may occur between slip events. Postseismic subcritical crack extension is not a process to which the constant stress boundary condition is appropriate: a process in which elastic strain is relaxed by permanent straining without further displacement is best described by boundary conditions which prescribe constant displacement; as would be met in experimental work by imposing a rapid displacement which is kept fixed while stresses are relaxed by permanent strains. No analysis is available for the appropriate crack type, i.e. Mode III, or even for Mode II cracks, but an analysis of Mode I cracks is given by Lawn & Wilshaw (1975). Whereas at constant force, equivalent to the constant stress condition, the crack-extension force (F) is an increasing function of crack length ($F \propto L^2$), at constant displacement the crack-extension force is a decreasing function of crack length ($F \propto L^{-4}$). Under constant displacement conditions Mode I cracks constitute a stable system and the amount of crack extension will not increase with the initial length of the crack. If Mode II and Mode III cracks have similar characteristics a constant slip increment would be feasible.

The significant material property determining subcritical crack extension for a given initial stress distribution is fracture toughness, values of which range from 0.3 MPa m^{-2} in poorly cemented sandstone to 3.6 MPa m^{-2} in fresh dunite (P. Meredith personal communication, 1986). High values of fracture toughness would correspond to low values of a, the slip increment, which displace growth curves to the left. As fault width is proportional to the square root of a and as the range of fracture toughness is no greater than one order of magnitude, variation in fracture toughness is likely to be of less significance than variation of shear modulus in determining the position of a fault on the D/W plot.

Das & Scholz (1981) have proposed a model for time-dependent subcritical crack growth which they show to be consistent with many characteristics of the earthquake mechanism, particularly aftershock sequences. The fault growth mechanism proposed here requires modification of the Das & Scholz model only to the extent of making crack extension independent of crack length.

For a constant rate of displacement of the regional boundaries the growth model requires that the number of active faults is reduced as individual faults become larger and that the recurrence time remains constant.

CONCLUSIONS

(1) A plot of W (width) against D (displacement) for normal faults and thrusts over a wide range of scales shows a linear trend on a log–log plot which is interpreted as a growth sequence.

(2) The data can be interpreted in terms of an arithmetic growth model in which the rate of increase of width of a fault is constant.

(3) Fault width is proportional to the square root of displacement, and the exact relationship is determined by material properties. The relevant material properties are shear modulus, fracture toughness and friction on the fault surface, of which shear modulus is the most significant.

(4) Radius/displacement ratios decrease systematically, but non-linearly, throughout the growth of a fault, from values characteristic of single slip events, *ca* 30,000, to about 500 on faults with displacements of 1 m and about 5 on faults with displacements of 40 km.

(5) Displacement/width data derived from single fault traces are affected by the position of the trace relative to the fault centre. The spread of data from fault traces on coalmine plans can be interpreted as the result of this geometrical effect, and of a variation in shear modulus of about half an order of magnitude (3–10 GPa).

(6) Synsedimentary faults may show growth curves which are steeper than the normal growth curve.

(7) Data on faults in Quaternary deposits are consistent with shear moduli about an order of magnitude lower (0.1 and 0.2 GPa) than the moduli of rocks from which other fault data are derived.

(8) The increase in dimensions of a fault is probably the result of postseismic, time-dependent, subcritical crack extension.

Acknowledgements—We thank John Mortimer and Iwan Williams for their assistance in extracting data from coalmine plans and in other ways, Philip Meredith for information and advice on fracture toughness and a reviewer for significant improvements to the manuscript. This paper is published with the permission of British Coal but the views expressed are those of the authors and not necessarily those of British Coal. The work was funded by British Coal and the European Coal and Steel Commission (contract Nos YCE.30/19572 and YCE.30/20214), the U.S. Earthquake Hazards Reduction Program (contract No. 14-08-0001-22072) and the Natural Environment Research Council (grant GR3/4719).

REFERENCES

Aitkenhead, N. 1985. Geology of the country around Buxton, Leek and Bakewell. *Mem. geol. Surv. Gt. Br.*, sheet 111.

Babenroth, D. L. & Strahler, A. N. 1945. Geomorphology and structure of the East Kaibab Monocline, Arizona and Utah. *Bull. geol. Soc. Am.* **56**, 107–150.

Barnett, J. A. M., Mortimer, J., Rippon, J. H., Walsh, J. J. & Watterson, J. 1987. Displacement geometry in the volume containing a single normal fault. *Bull. Am. Ass. Petrol. Geol.* **71**, 925–937.

Barrientos, S. E., Ward, S. N., Gonzalez-Ruiz, J. R. & Stein, R. S. 1985. Inversion for moment as a function of depth from geodetic observations and long period body waves of the 1983 Borah Peak, Idaho Earthquake. In: *Proceedings of Workshop XXVII on the Borah Peak, Idaho, Earthquake* (edited by Stein, R. S. & Buckham, R. C.). *U.S. Geol. Surv. Open File Report* 85–290, 485–518.

Beck, E. 1929. Salt Creek oil field, Natrona County, Wyoming. In: *Structure of typical American Oil Fields*, Vol. II. Am. Ass. Petrol. Geol. 589–603.

Birch, F., 1966, Compressibility; elastic constants. In: *Handbook of Physical Constants* (edited by Clark, S. P.). *Geol. Soc. Am.* Memoir **97**, 97–173.

Bond, D. C., Atherton, E., Bristol, H. M., Buschbach, T. C., Stevenson, D. L., Becker, L. E., Dawson, T. A., Fernalld, E. C., Schwalb, H., Wilson, E. N., Statler, A. T., Stearns, R. G. & Buehner, J. H. 1971. Possible future petroleum potential of Region 9—Illinois Basin, Cincinnati Arch, and Northern Mississippi Embayment. In: *Future Petroleum Provinces of the United States—Their Geology and Potential* (edited by Cram, I. H.). *Am. Ass. Petrol. Geol.* Memoir **15**, 1165–1218.

Brunstrom, R. G. W. 1963. Recently discovered oilfields in Britain. In: *Proceedings of the 6th World Petroleum Congress—Section I*, Verein zur Forderung, Hamburg, 11–20.

Cave, R. 1977. Geology of the Malmestry District. *Mem. geol. Surv. Gt Br.*, sheet 251.

Coward, M. P. & Potts, G. J. 1983. Complex strain patterns developed at the frontal and lateral tips to shear zones and thrust zones. *J. Struct. Geol.* **5**, 383–393.

Das, S. & Scholz, C. H. 1981. Theory of time dependent rupture in the earth. *J. geophys. Res.* **86**, 6039–6051.

Drozdzewski, V. G. 1980. Tiefenteknik der Emscher- und Essener-Hauptmulde im mittleren Ruhrgebiet. In: *Beitrage zur Tieftektonik des Ruhrkarbons*. Geologisches Laudesaint Nordrein-Westfalen, Krefeld, 45–83.

Elliott, D. 1976. The energy balance and deformation mechanisms of thrust sheets. *Phil. Trans. R. Soc. Lond.* **A283**, 289–312.

Frost, D. V. & Smart, J. G. O. 1979. Geology of the country north of Derby. *Mem. geol. Surv. Gt Br.*, sheet 125.

Frost, D. V. & Halliday, D. W. 1980. Geology of the country around Bellingham. *Mem. geol. Surv. Gt Br.*, sheet 13.

Huntoon, P. W. 1974. The post-Palaeozoic structural geology of the Eastern Grand Canyon, Arizona. In: *Geology of the Grand Canyon*. Museum of Northern Arizona and Grand Canyon Natural History Association, Arizona, 82–115.

Janoschek, R. H. & Gotzinger, K. G. H. 1969. Exploration for oil and gas in Austria. In: *The Exploration for Petroleum in Europe and North Africa* (edited by Hepple, P.). Elsevier, Amsterdam, 161–180.

Kanamori, H. & Anderson, D. L. 1975. Theoretical basis of some empirical relations in seismology. *Bull. seism. Soc. Am.* **65**, 1075–1095.

Kasahara, K. 1981. *Earthquake Mechanics*. Cambridge University Press, Cambridge, U.K.

Lambe, T. W. & Whitman, R. V. 1969. *Soil Mechanics*. John Wiley, New York.
Lawn, B. R. & Wilshaw, T. R. 1975. *Fracture of Brittle Solids*. Cambridge University Press, Cambridge, U.K.
Mayuga, M. N. 1970. Geology and development of California's Giant-Willmington Field. In: *Geology of Giant Petroleum Fields* (edited by Halbouty, M. T.). *Am. Ass. Petrol. Geol.*, Memoir **14**, 158–184.
Muraoka, H. & Kamata, H. 1983. Displacement distribution along minor fault traces. *J. Struct. Geol.* **5**, 483–495.
Nelson, P. H. H. 1980. Role of reflection seismic in development of Nembe Creek Field, Nigeria. In: *Giant Oil and Gas Fields of the Decade*: 1968–1978 (edited by Halbouty, M. T.). *Am. Ass. Petrol. Geol.*, Memoir **30**, 565–576.
Reeves, J. R. 1929. El Dorado oil field, Butler County, Kansas. In: *Structure of Typical American Oilfields*, Vol. II. *Am. Ass. Petrol. Geol.*, 160–167.
Rippon, J. H. 1985. Contoured patterns of the throw and hade of normal faults in the Coal Measures (Westphalian) of north-east Derbyshire. *Proc. Yorks. geol. Soc.* **45**, 147–161.
Ruppel, E. T. 1982. Cenozoic block uplifts in east-central Idaho and southwest Montana. *U.S. Geol. Surv. Professional Paper*, 1224.
Scholz, C. H. 1982. Scaling laws for large earthquakes; consequences for physical models. *Bull. seism. Soc. Am.* **72**, 1–14.
Scholz, C. H., Aviles, C. A. & Wesnousky, S. G. 1986. Scaling differences between large interplate and intraplate earthquakes. *Bull. seism. Soc. Am.* **76**, 65–70.
Scott, W. E., Pierce, K. L. & Halt, M. H. Jr. 1985. Quaternary tectonic setting of the 1983 Borah Peak earthquake, central Idaho. In: *Proceedings of Workshop XXVIII on the Borah Peak, Idaho, Earthquake* (edited by Stein, R. & Buckham, R. C.). *U.S. Geol. Surv. Open File Report* 85–290, 1–16.
Shepherd, J. & Burns, K. L. 1978. Fault swarms in the Greta Coal Seam, New South Wales. *Proc. Australas. Inst. Min. Metall.* **267**, 27–36.
Shoemaker, E. M., Squires, R. L. & Abrams, M. J. 1978. Bright Angel and Mesa Butte fault systems of northern Arizona. In: *Cenozoic Tectonics and Regional Geophysics of the Western Cordillera* (edited by Smith, R. B. & Eaton, G. P.). *Geol. Soc. Am.* Memoir **152**, 341–367.
Stein, R. S. & Barrientos, S. E. 1985. The 1983 Borah Peak, Idaho, Earthquake: Geodetic evidence for deep rupture on a planar fault. In: *Proceedings of Workshop XXVIII on the Borah Peak, Idaho, Earthquake* (edited by Stein, R. S. & Buckham, R. C.). *U.S. Geol. Surv. Open File Report* 85–290, 459–484.
Teas, L. P. 1929. Bellevue oil field, Bossier Parish, Louisiana. In: *Structure of Typical American Oilfields*, Vol. II. *Am. Ass. Petrol. Geol.*, 229–253.
Tschopp, R. H. 1967. Development of the Fahud Field. In: *Proceedings of the 7th World Petroleum Congress*, Vol. 2. Elsevier, Amsterdam, 231–242.
Van den Bark, E. & Thomas, O. D. 1980. Ekofisk: First of the Giant Oil Fields in Western Europe. In: *Giant Oil and Gas Fields of the Decade*: 1968–1978 (edited by Halbouty, M.T.). *Am. Ass. Petrol. Geol.*, Memoir **30**, 195–224.
Verdier, A. C., Oki, A. C. & Suardy, A. 1980. Geology of the Handil Field (East Kalimanton–Indonesia). In: *Giant Oil and Gas Fields of the Decade*: 1968–1978 (edited by Halbouty, M. T.). *Am. Ass. Petrol. Geol.*, Memoir **30**, 399–421.
Wallace, R. E. 1985. Variations in slip rates, migration and grouping of slip events on faults in the Great Basin Province. In: *Proceedings of Workshop XXVIII on the Borah Peak, Idaho, Earthquake* (edited by Stein, R. S. & Buckham, R. C.). *U.S. Geol. Surv. Open File Report* 85–290, 17–26.
Walsh, J. J. & Watterson, J. 1987. Distribution of cumulative displacement and of seismic slip on a single normal fault surface. *J. Struct. Geol.* **9**, 1039–1046.
Watterson, J. 1986. Fault dimensions, displacements and growth. *Pure & Appl. Geophys.*, **124**, 365–373.

APPENDIX

On a fault growing according to the arithmetic growth model, with last slip u_n, cumulative displacement D, and radius R, and with n slip events, if successive slips $u_1, u_2, u_3 \ldots, u_n$ have common difference, a, and first term zero, then

$$u_n = a \times (n - 1)$$

when n is large

$$u_n = a \times n. \tag{A1}$$

Displacement, D, is the sum of all slips and when the first term of the summation is zero,

$$D = n/2 \times (n - 1) \times a;$$

when n is large

$$D = (n^2 \times a)/2 \tag{A2}$$

from (A1)

$$n = u_n/a$$

and

$$n^2 = u_n^2/a^2.$$

Combining equations (A1) and (A2),

$$D = (u_n^2/a^2) \times a/2$$
$$D = (u_n^2/a)/2 = u_n^2/2a$$

or

$$u_n = (2 \times a \times D)^{1/2} \tag{A3}$$

for a single earthquake slip event, stress drop ($\delta\sigma$) and rigidity modulus (G) are related to u_n and R by the following expression (Kanamori and Anderson 1975)

$$\delta\sigma = (7 \times \pi \times G/16) \times u_n/R, \tag{A4}$$

where $7 \times \pi/16$ is the shape factor for a circular fault.

$$R = (7 \times \pi \times G \times u_n)/(16 \times \delta\sigma).$$

If

$$k = (7 \times \pi \times G)/(16 \times \delta\sigma)$$

then

$$R = k \times u_n. \tag{A5}$$

Combining (A4) and (A5)

$$R = k \times (2a \times D)^{1/2} \tag{A6}$$
$$W = 2R = 2k \times (2a \times D)^{1/2}$$
$$W^2 = 4 \times k^2 \times 2 \times a \times D$$
$$W^2 = k^2 \times 8 \times a \times D.$$

$W^2 = P \times D$ which is equation (1) in the text, where

$$P = k^2 \times 8a$$

or

$$P = ((7 \times \pi \times G)/(16 \times [\delta\sigma]))^2 \times 8a \tag{A7}$$

so

$$W^2 = D \times ((7 \times \pi \times G)/(16 \times [\delta\sigma]))^2 \times 8a, \tag{A8}$$

i.e. the value of P is dependent on the variables G, $\delta\sigma$ and a.